Kinetic Analysis and Probability Mapping Applied to the Detection of Ovarian Cancer by Radioimmunoscintigraphy

Maria Granowska, Cyril C. Nimmon, Keith E. Britton, Mary Crowther, Steve J. Mather, Maurice L. Slevin, and John H. Shepherd

St. Bartholomew's Hospital and Medical College, University of London; and Imperial Cancer Research Laboratories, London, UK

Kinetic analysis with probability mapping is an objective method of serial image analysis applicable to radioimmunoscintigraphy. The technique is described and subjected to clinical testing by comparing the prediction of biopsy histology from the probability map in patients coming to operation. In those with ovarian cancer undergoing second-look laparotomy after completing full courses of chemotherapy, the prediction of histology in 108 biopsy sites was 45 true positives and 38 true negatives, sensitivity 80%, specificity 73%, accuracy 77% $p < 0.001$. In patients with tumors <2 cm diameter, 41 biopsy sites were predicted with a specificity of 78% and an accuracy of 76%, $p < 0.01$. The technique is reducing the need for second-look laparotomy in patients with subclinical and subradiological disease. Such disease is suitable for intraperitoneal radioimmunotherapy.

J Nucl Med 29:599–607, 1988

If radioimmunoscintigraphy (RIS) is to solve patient management problems that are not amenable to conventional techniques, then it has to be able to detect subclinical and subradiological disease. Since the technique makes use of the intrinsic properties of the cancer cell and not the shape, size, or placement of the malignancy as demonstrated radiologically, it has the potential of high specificity and high detectability. However, currently available radiolabeled antibodies are rather poor radiopharmaceuticals with rarely better than 0.1% of the injected dose taken up per gram and more usually 0.01% per gram. Therefore, efforts have to be made to improve tumor detectability by increasing the signal and reducing the noise around the target.

The technical problem has been approached by using the short-lived radionuclide iodine-123 (^{123}I) which has a high count rate capability with the highly avid monoclonal antibody HMFG2 (Human milk fat globule second antibody), and by developing and applying a new algorithm for RIS image analysis: kinetic analysis with probability mapping to enhance the specificity of small tumor detection. The basis of this differentiation of tumor from other tissue is that tumor uptake of the specific antibody increases with time, whereas the blood pool, nonspecific uptake, and other tissue activity decreases with time after the initial distribution. Thus, if a series of images are taken over a period of time and then analyzed in such a way as to combine the temporal change, together with the count rate distribution, tumor sites should be clearly identifiable. The clinically important context is that of predicting whether or not abdominal tumor persists or has recurred after the completion of full courses of chemotherapy following the primary operation for ovarian cancer.

Second look operation is routinely applied in this hospital for therapeutic assessment. This enabled an objective biopsy-based determination of the efficacy of the detection technique with the goal of reducing or obviating the need for second surgery in these patients.

The aim of this study is to compare prospectively the results of RIS with data processing using kinetic analysis and probability mapping with the subsequent results of surgery and the biopsy findings. A preliminary report of this work has been given to the NATO Advanced Scientific Institute Meeting. (*1*)

Received June 1, 1987; revision accepted Nov. 12, 1987.

For reprints contact: Maria Granowska, MD, Dept. of Nuclear Medicine, St Bartholomew's Hospital Medical College, West-Smithfield, London EC1A 7BE.

MATERIALS AND METHODS

Antibody

The monoclonal antibody HMFG-2 is an epithelial specific, tumor-associated antibody of class IgG1. The hybridoma-

producing HMFG-2 was derived from the fusion of the mouse myeloma cell line NSI with the spleen cells of a mouse which has received an initial injection of human milk fat globule (HMFG) followed by a boost with cultured normal milk epithelial cells (*2*). By immunoperoxidase staining of formalin-fixed, paraffin-embedded sections, the spectrum of reactivity of the antibody has been determined (*3*). It reacts with primary and metastatic breast tumor, ovarian cancer, and colonic cancer and weakly with the normal epithelial cells of these tissues. It also reacts with some cervical cancers and some other adenocarcinomata.

The antigenic determinant is carried on a high molecular weight (300 k) glycoprotein (*4*) containing at least 50% carbohydrate (*5*) and is present in low density on the epithelial surfaces of secretory tissues but in higher numbers in the cell membranes of many tumors, particularly those of breast and ovarian origin (*3,5*).

Labeling with ^{123}I

Iodine-123 has an ideal energy (159 keV) for the gamma camera and a half-life of 13.2 hr which allows a count rate to be obtained of ~20 times that of iodine-131 for the same administered activity and for a lower absorbed radiation dose. Iodine-123 is supplied dissolved in sodium hydroxide in sterile vials (Atomic Energy Research Establishment, Harwell) free of iodine-124 and with <0.02% of iodine-125. The iodogen reaction is used with ^{123}I to label the monoclonal antibody. The iodogen is dissolved in dichloromethane to make iodogen solution and evaporated to dryness at 37°C in sterile propylene tubes. Iodogen reagent then coats the inside of the tube and these tubes can be stored at 5°C for 6 mo without loss of reactivity. For labeling pure ^{123}I, the mouse monoclonal antibody, 1–2 mg/ml in $10^{-5}M$, Tris buffer, pH 7.4 and potassium iodide, $4 \times 10^{-4}M$ in water are mixed in the iodogen tube. The mixture is left at room temperature for 10 min with gentle shaking and then decanted on to a Sephadex G-50 filtration column in a 20-ml syringe prewashed with 1% human serum albumin in phosphate-buffered saline. After a 5-ml void volume, the eluate is collected in 2-ml aliquots, activity assayed and passed through a micropore filter into sterile vials. Using appropriate quality control, it is found that the labeling efficiency is typically over 70%. Reactivity of iodinated antibody with breast cancer cells is tested using enzyme-linked immunosorbent assay (ELISA) and by direct radioimmunoassay. It is shown that this iodogen method leaves the active center of the antibody intact with its avidity unaltered.

Patient Selection

The approval of the City & Hackney District Ethical Committee and the Administration of Radioactive Substances Advisory Committee was obtained. There were two groups of patients: those presenting with a pelvic mass suspected to be ovarian cancer were studied before their first operation; and those having complete chemotherapy for ovarian cancer were imaged before their second look operation. Their ages were between 30 and 75 yr of age and they were under the care of the gynecologist (J.S.). The procedure was explained and each gave signed consent. Potassium iodine 60 mg b.d. was given orally the day before, on and for 3 days after the study, and 400 mg potassium perchlorate on the morning of the study. A history of allergy, particularly to foreign protein, was taken and if positive the patient was excluded (one case). An intradermal skin test with 0.1 ml containing 50 μg of the unlabeled antibody, with a saline control on the opposite arm, was performed at least 30 min before the study and a wheal >2 cm diameter was considered positive, the patient again being excluded (no cases).

Patients were sent to the department with the clinical information only that they might have primary or secondary ovarian cancer in the abdomen. No other clinical, radiological, operative, or laboratory information was provided until the end of the study after the time that the decisions on the image and the results of image analysis were made.

The patient was positioned comfortably supine on the imaging couch. A Siemens ZLC 37 photo-tube camera (Searle-Siemens, Medical Systems, Inc., Iselin, NJ), fitted with a high resolution, parallel hole, collimator designed for up to 200-keV energy gamma rays, was placed anteriorly over the patient's pelvis. The system was peaked for ^{123}I 159 keV with a 20% window. The injection of 2–3 mCi (80–120 MBq) of [^{123}I]HMFG2 containing 0.4 mg of monoclonal antibody was administered intravenously into the right antecubital vein. Dynamic studies were recorded at a 30-sec framing rate for the first 10 min directly on line into the DEC gamma 11 computer. Static images were taken at 10 min, at 4 hr and at 22 hr anteriorly and posteriorly over the lower part of the chest, the abdomen, and the pelvis together with separate marker scans. For the latter, the patient's bony landmarks, xiphisternum, costal margins, anterior superior iliac spines, and symphysis pubis were marked with indelible ink, and point source radioactive markers were positioned over these six sites. Transparent films of the marker positions on the persistence scope were made at the early visit. At each subsequent visit, the markers were repositioned on the patient, and the patient was repositioned until the image of the marker on the persistance scope fitted that on the previously recorded film positioned over the scope. Digitized images of the markers were recorded on the computer and a special program was used to align the corresponding patient image data using corrections for both translation and rotation. This alignment procedure allows detailed computer analysis of the images to be performed subsequently (see Appendix). After completion of the 22-hr images, the patient underwent surgery.

Data Assessment

After completion of the image analysis probability maps identifying the sites of significant positive change in uptake between the 10-min and 22-hr images were reviewed for each patient. Specific uptake in tumor sites are demonstrated by this means but certain other changes will be seen in addition. These include probably nonspecific increased accumulation of this whole IgG antibody in the liver and spleen with time, and the accumulation of metabolic products, for example free iodine, will show an increase in the urinary systems and on occasion in the stomach with time. However, such accumulation in these normal structures is not usually mistaken for sites of pathologic uptake and decisions are made as to which parts of the images are due to these processes and which are pathologic sites of increasing antibody uptake.

At surgery each location of tumor and a series of up to 14 biopsies at different sites are taken to look for microscopic disease. A list of these sites was then presented by the surgeons without histologic or other details, to the imaging physicians, who then had to call each site in each patient as positive or

negative, from the probability map. It should be noted that the specification of the site of biopsy was sometimes imprecise such as "left paracolic gutter" or "omentum". However, the exercise was undertaken as rigorously as possible. As well as the location of positive or negative sites, a record was made if sites other than those biopsied were image positive and an overall statement was made for the images as to whether or not the patient was tumor free or had residual disease. After completion of this exercise, the histology was given by the surgeon and the probability map was scored as being correct or incorrect in tumor location and in overall assessment. Statistical assessment was by the chi-squared test comparing the observed scoring of the probability map for each biopsy site: tumor present or absent, with the histologic findings. A probability value of $p < 0.05$ was considered a significant and $p < 0.001$ highly significant association.

RESULTS

The comparison of the readings of the probability maps at the stated biopsy sites and the final histologic demonstration of whether the biopsy was positive for tumor or negative is shown in Table 1 for patients undergoing their first operation and in Table 2 for patients having a second-look laparotomy. The results are displayed according to biopsy site. In Table 1 there were 19 true positives, (TP), six false negatives, (FN), 10 true negatives and eight false positive results from the ten patients undergoing their first operation. Chi squared equals 4.5 which is significant, $p < 0.05$. In Table 2 there were 45 true positives, 11 false negatives, 38 true negatives and 14 false positives from the 21 patients coming to second-look operation. Chi-squared equals 31.3 which is highly significant, $p < 0.001$. The combined chi-squared value for the 31 patients is 34.7 also highly significant, $p < 0.001$. There were ten patients whose findings at surgery showed either a tumor or tumors of <2 cm diameter or no abnormality at second-look operation (Patients 14, 16, 17, 19, 20, 21, 23, 25, 27, and 30). Taking these results alone, chi-squared equals 7.4 which is significant, $p < 0.01$.

Some case reports illustrate the best and worst results of the application of kinetic analysis with probability mapping to radioimmunoscintigraphy.

Patient 27

A 51-yr-old woman presented previously with a poorly differentiated serous adenocarcinoma of the ovary, Stage III. After successful primary surgery, she received full courses of chemotherapy. She showed no physical or radiological (x-ray CT) abnormality at the time of second-look surgery. Apart from stomach and bladder activity the probability map was reported to be normal for all biopsy sites which showed no histologic abnormality—a true-negative result (Fig. 1).

Patient 24

A 67-yr-old woman presented with a central pelvic mass shown at the first operation to be due to a serous adeno carcinoma. She underwent full courses of chemotherapy but a residual pelvic mass was evident clinically and radiologically. Radioimmunoscintigraphy findings are shown in Figure 2. The extent of metastases is difficult to determine from the simple subtraction image (22-hr image minus 10-min image—bottom left). The widespread distribution of tumor in the abdomen is clearly shown on the probability map ($p < 0.001$) for positive change between the two images in black). Biopsy sites in the left and right ovaries, omentum and mesentery, left and right paracolic regions were all correctly called positive.

Patient 30

A 54-yr-old woman had a poorly differentiated serous adenocarcinoma successfully removed at first operation, followed by full courses of chemotherapy. No clinical or radiological (x-ray CT) evidence of tumor was found. Probability mapping from RIS before the second-look operation showed positive uptake at sites in the upper abdomen, called positive for the mesentery site that was biopsied (correct) and no other abnormality; biopsy of the uterus, which was suspicious at surgery, being negative (correct) (Fig. 3).

Patient 8

A 46-yr-old woman presented with a pelvic mass demonstrated to be a Stage III carcinoma of the cervix with a large right ovarian metastasis at primary surgery. The results of the comparison of the 10-min and 22-hr images by kinetic analysis with probability mapping are shown in Figure 4. Areas in black show highly significant positive uptake ($p < 0.001$) occurring between the early and late images on the anterior image. Activity in the pelvis is noted and on the posterior view the mass uptake is seen superior to the bladder activity. Edge artifact activity is seen around the liver with small sites of activity to the left of the mid-line in relation to the liver, prominent on the posterior view image. The image was interpreted as positive for uterine uptake (correct) and for left ovarian uptake (incorrect); negative for right ovarian uptake (incorrect); negative for uptake in the appendix (correct) and positive for para-aortic lymph nodes (incorrect). This represents a "worst case" example, probably because at the time of imaging the right ovarian mass was lying in the mid-line.

DISCUSSION

The assessment of ovarian cancer after the completion of full courses of chemotherapy is such a difficult problem that a second look laparotomy is performed routinely in many centers. It is performed for two main reasons: to debulk clinically and radiologically evident tumors and to detect subclinical and subradiological disease both visually and through multiple biopsies of likely sites of recurrence. The detection of recurrence under two centimeters is difficult by ultrasound and x-ray CT because of the interpretation of overlapping and/or inherent loops of bowel and because postsurgical or therapy fibrosis cannot be easily distinguished from tumor recurrence (*6,7*).

Conventional radioimmunoscintigraphy also has difficulties in detecting small areas of residual disease. Results obtained using transparent picture display may

Key to Tables 1 and 2

Scoring (+) tumor present;
(−) tumor not present.
Upper sign, map report;
Lower sign, biopsy finding for each site.

Sites of biopsy
U: Uterus CP.
LO: Left ovary/Left central pelvis.
RO: Right ovary/Right central pelvis.
LIL: Left infundibular ligament.
RIL: Right infundibular ligament.
V: Vaginal vault.
O: Omentum.
A: Appendix.
M: Mesentery of small intestine.
LPC: Left paracolic region.
RPC: Right paracolic region.
L: Liver.
LD: Left subdiaphragmatic region.
RD: Right subdiaphragmatic region.
PAR: Para-aortic region.
POD: Pouch of Douglas.
PW: Peritoneal washings/ascites.

Differentiation Mod, moderately;
Well; Poor; Undiff, Undifferentiated.

Histology Endo, Endometrial cancer;
Ser Pap, Serous Papillary Carcinoma;
Muc, Mucinous adenocarcinoma;
Ben, Benign;
Ca Sarc, Carcinosarcoma;
Muc Cyst, Mucinous Cystadenoma;
Adeno ca, Adenocarcinoma:
Mull Mesosarc, Mullerian Mesosarcoma;
( ), Original tumor histology, no residual tumor on biopsy.

Outcome TP: True positive;
FN: False negative;
TN: True negative;
FP: False positive.

have insufficient contrast and resolution for the purpose (*8,10*). Count rates may be too low for adequate single photon emission tomography. The use of a second radiopharmaceutical with a radionuclide of different energy to undertake background subtraction leads to artifacts due to different tissue attenuations and distributions, particularly when small lesions are sought (*9*). Improving the signal through the use of ^{123}I as the radiolabel has improved the detectability of moderate sized recurrences with 90% accuracy in a prospective study (*10*) but not disease <1 cm diameter.

Apart from a second-look laparotomy indicating the need for further chemotherapy, the introduction of intraperitoneal radioimmunotherapy, RIT, (*11*) has given further impetus to the demonstration of residual disease under 2 cm diameter, for it appears that only patients with ascites or with disease in this range show benefit. It is also essential to demonstrate that the tumor has the appropriate antigenic structure able to bind the antibody in vivo, for in our experience of 13 patients considered for RIT, one with in vitro immunoperoxidase staining evidence of antibody binding was negative on radioimmunoscintigraphy.

The task then is to develop a technique of radioimmunoscintigraphy that can meet this challenge. In order to improve the method of background subtraction, we introduced the technique of subtracting an early image, taken at 10 min, from the later image (*12,13*). The early image shows the distribution of tissue and blood background distribution at a time when there is relatively little specific tumor uptake. Tissue and blood background and some nonspecific uptake tends to decrease with time. This late minus early subtraction

TABLE 1
First Operation: Biopsy and Surgical Site Histology Compared with Prior RIS Diagnosis

Patient	Histology	U	LO	RO	LIC	RIC	V	O	M	A	LPC	RPC	L	LD	RD	PAR	POD	PW	Outcome			
																			TP	FN	TN	FP
1	Benign thecoma	+	+	−				+		+											1	4
		−	−	−				−		−												
2	Undiff			+			+	+	+	−	+								5	1		
				+			+	+	+	+	+											
3	Poor ca sarc	+	+	+	−			−	−	+							−		4	3	1	
		+	+	+	−			+	+	+							+					
4	Liposarcoma															+			1			
																+						
5	Poor ser pap		+	+				+			+		+						5			
			+	+				+			+		+									
6	Ben muc cyst	−	−	−																	3	
		−	−	−																		
7	Fibroid	+	−	−																	2	1
		−	−	−																		
8	Cervix adenoca	+	+	−						−						+			1	1	1	2
		+	−	+						−						−						
9	Fibroid	+	−	−																	2	1
		−	−	−																		
10	Mull mesosarc	+	+	+				−											3	1		
		+	+	+				+														
																Total			19	6	10	8

TABLE 2
Second Look Operation: Biopsy Site Histology Compared with Prior RIS Diagnosis

Patient no.	Histology	U	LO	RO	LIL	RIL	V	O	M	A	LPC	RPC	L	LD	RD	PAR	POD	PW	Outcome			
																			TP	FN	TN	FP
11	Mod endo				−		+	+											1	1		1
					+		+	−														
12	Well serous	+	−	+				−	+	−									2	1	2	1
		+	+	+				−	−	−												
13	Mod serous				+	+	+		+		+	−		+	+				7	1		
					+	+	+		+		+	+		+	+							
14	(Mod muc)							−		+											1	1
								−		−												
15	Mod ser pap	+	+	+	+			+		+				+	+				7			1
		+	+	+	+			+		+				−	+							
16	Poor serous				+			+				+						+	1			3
					+			−				−						−				
17	Mod serous							+											1			
								+														
18	Poor serous	−	+	+				−				+	−			+		+	4	3		1
		+	+	+				+				+	+			−		+				
19	Poor serous				−		+						−	−			+	−		1	3	2
					+		−						−	−			−	−				
20	Poor ser pap					+	+	−			−								1	2		1
						−	+	+			+											
21	(Undiff)		−	−														−			3	
			−	−														−				
22	Mod serous		+	+														+	2			1
			+	−														+				
23	Well muc						+	−		−	−	−	+						2		4	
							+	−		−	−	−	+									
24	Mod serous		+	+				+	+		+	+							6			
			+	+				+	+		+	+										
25	(Mod serous)				−	−			−		−	−		−	−		−				8	
					−	−			−		−	−		−	−		−					
26	Poor muc				+		+		−	+		+	−				+	+	4		2	2
					−		−		−	+		+	−				+	+				
27	(Poor serous)				−	−		−			−	−									5	
					−	−		−			−	−										
28	Poor serous			+					−								−		1		2	
				+					−								−					
29	Mesonephroid	+			−	−		+	−				+				+		4	2	1	
		+			+	−		+	+				+				+					
30	Poor serous	−							+										1		1	
		−							+													
31	Well ser pap	−							−		−	−			+	−		−	1		6	
		−							−		−	−			+	−		−				
															Total				45	11	38	14

procedure certainly enhances sites of residual disease as in Figure 2. There are two main problems; the patient must be repositioned reasonably accurately and then precise superimposition of the images must be performed; and image normalisation is required. Taking care particularly to avoid torsion of the patient and using the patient repositioning protocol described under Methodology, at each visit for imaging with six markers, suitable marker and abdominal images can be obtained for their further computer aided superimposition. The translation, rotation algorithm for this is described in Appendix 1.

The marker images are first analyzed to find the most active pixels at each marker site and then the steps to superimpose the pair of early and late marker images are undertaken. Once this is achieved the early and late abdominal images are put through the same steps. It can be easily appreciated if the technique is not successful, for shadowing of the blood vessels is seen on the subtraction image.

The normalization procedure for this simple subtraction approach can never be rigorous since the later distribution contains differences in distribution of activity for the former. Conventional procedures such as normalizing each image to total count, to maximum count or to counts from a region of interest which appears not to have changed may be performed and this latter is reasonably successful. Alternatively, serial subtraction of increasing proportions of the count rate distribution of the early from late image may be controlled by the operator, who chooses a "best looking" image. However, under-subtraction will tend to en-

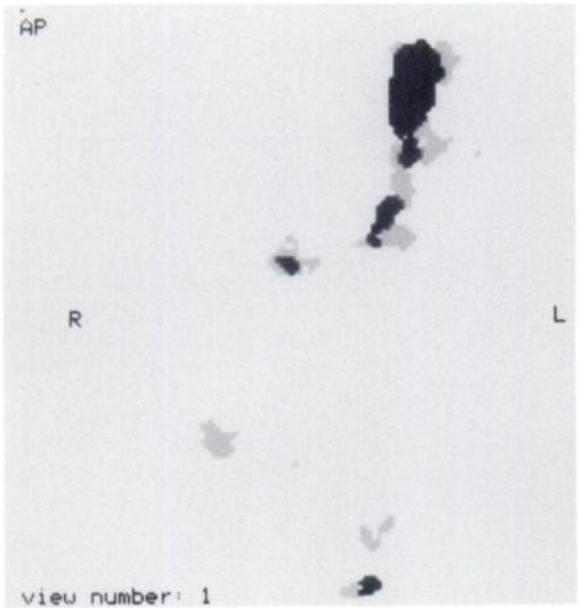

FIGURE 1
Patient 27: Anterior abdominal probability map after kinetic analysis of the 10-min and 4-hr images. Pixels showing significant positive changes at the $p < 0.001$ level are shown in black. Only stomach and bladder activity due to free ^{123}I were thought highly significant. The map was reported negative for five biopsy sites correctly.

hance "noise blobs" and over-subtraction will tend to lose sites of specific uptake so this approach is subjective. However, combining both of the above approaches is quite efficient.

In order to attempt this subjective element and operator dependence, an objective approach called kinetic analysis with probability mapping was developed by Cyril Nimmon (*9,13*). This approach identifies and places a statistical significance upon positive and negative changes in the distribution of activity between two images on a pixel by pixel basis. Originally conceived for comparing serially the uniformity fields in response to a flood source of a gamma camera, its application to pairs of a series of images to detect changes, typically temporal changes, between them has been dramatic on occasion, and is of potentially widespread application to nuclear medicine and other serial imaging procedures. The approach is given in more detail in the Methodology section and the algorithm in Appendix 2.

We report here its use in a prospective study suspected ovarian disease with histological control. Patients with pelvic masses coming to operation for the first time showed less encouraging results because of the positive identification of a range of tumors which were not ovarian cancer due to the cross-reactivity of the antibody, giving a specificity of only 56% and sensitivity of 76%. The results are shown in Table 1.

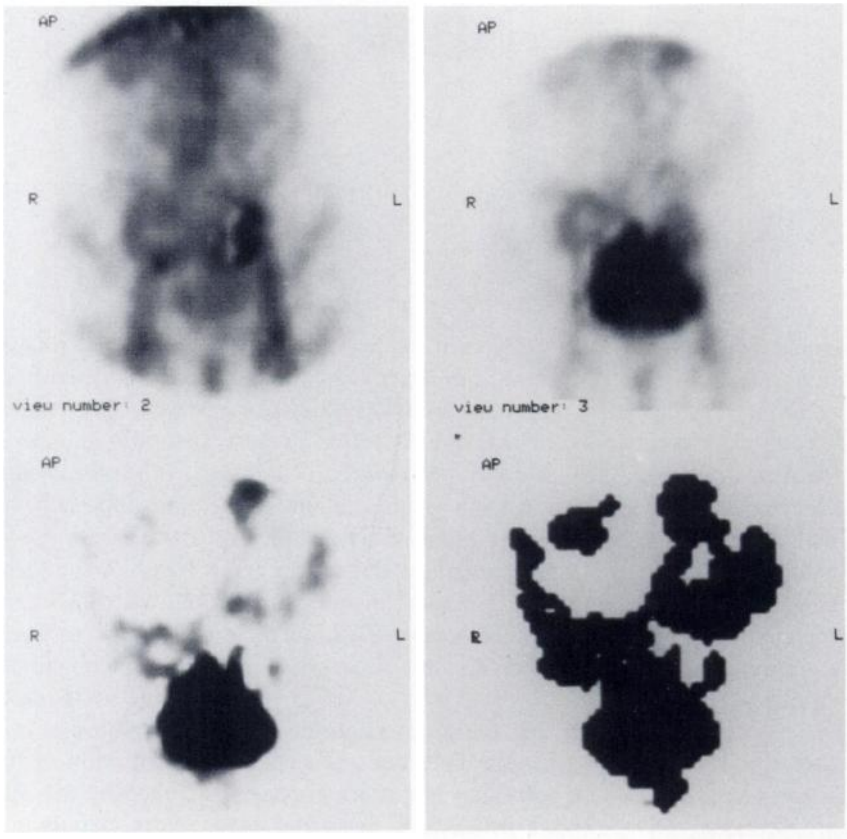

FIGURE 2
Patient 24: Anterior abdominal RIS images at 10 min, top left; 22 hr, top right. Subtraction image (22 hr minus 10 min), bottom left; Probability map bottom right; with pixels showing positive change between the two images at the $p < 0.001$ level in black. A greater extent of tumor involvement of the abdomen is demonstrated by the probability map as compared to the simple subtraction map.

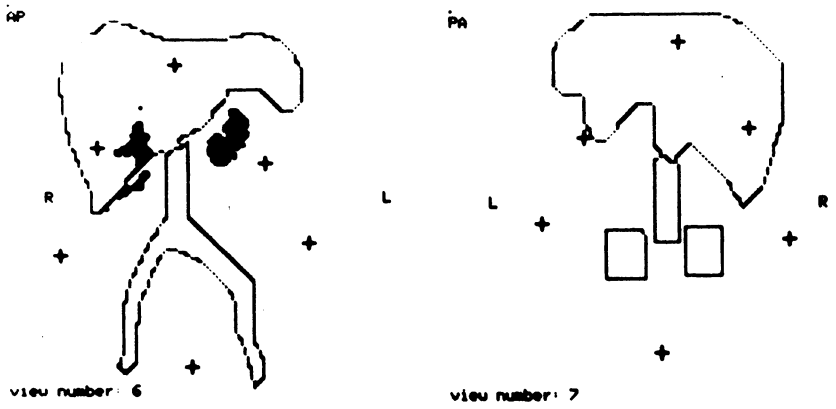

FIGURE 3
Patient 30: Probability maps of the abdomen; anterior, left; posterior, right with outlines of the organs and vessels drawn from the computer displayed images. (+) signs indicate bone landmarks (costal margin, xiphisternum and iliac crests). Pixels showing positive changes between the 10-min and 4-hr images with $p < 0.001$ are shown in black. Uptake and three sites in the upper abdomen are seen on the anterior view. The posterior view is clear making the sites of positive uptake on the anterior view unlikely to be renal, for no bladder or stomach activity is seen. The mesentery biopsy site was predicted correctly to be positive from the map and other uterine sites correctly predicted to be negative.

The results are better in the key clinical problem of determining recurrence after chemotherapy. Before second look laparotomy 108 biopsy specimens were analyzed and the probability map scored as tumor present or absent for the biopsy site and then this was compared with the histology. A sensitivity of 80%, specificity of 73% and accuracy of 77% was obtained. It should be noted that this was accuracy for localization of disease and the main problem in this study was the relative lack of precision by the surgeon in describing the exact site of the biopsy. Terms such as "omentum", "mesentery", "paracolic gutter", cover a large area and it is felt that this is one of the main causes for the lack of accuracy. Change in organ position between imaging and laparotomy under anesthetic may also contribute as may be the case in Figure 4. Nevertheless, when the data is re-analyzed for those patients with disease under 2 cm diameter (ten patients, 41 biopsy sites), a specificity of 78% and an accuracy of 76% was obtained. Three out of four disease-free patients as assessed by laparotomy and biopsy were correctly identified.

There are two problems of interpretation with probability mapping. Firstly, as well as specific tumor uptake, some other sites show a significant increase with time. With ^{123}I these are the bladder and the stomach even with prior preparation of the patient with potassium iodide and perchlorate. However, these normal sites are usually easily identified with reference to the unprocessed images. However, if bowel secretion of the antibody occurs, as for example with ^{111}In-labeled anti-carcino embryonic antigen, normal movement of bowel content between the early and later image will show up as false positive sites on the map. This means that this approach is not applicable in such situations.

In conclusion, we have demonstrated that this new technique of kinetic analysis with probability mapping has a specific application in radioimmunoscintigraphy where the clinical problem is the detection of subclinical and subradiological disease, in this case after completing courses of chemotherapy in ovarian cancer.

It is felt that given the immense effort to develop, make, charaterise, select, purify and radiolabel monoclonal antibodies, an equivalent effort should be made to improve radioimmunoscintigraphy by data analysis so that disease not detectable by other techniques may be demonstrated and thereby alter clinical manage-

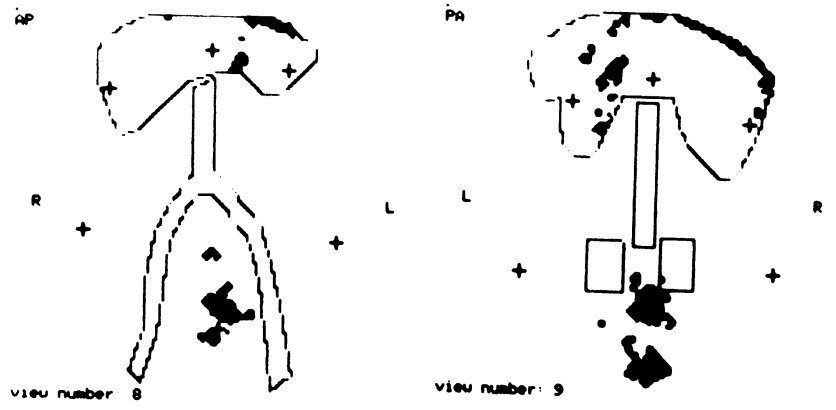

FIGURE 4
Patient 7: Probability maps of the abdomen (key as for Fig. 3). Pixels showing the positive changes between the 10-min and 22-hr image with a $p < 0.001$ are shown in black. An abnormality superior to the bladder is indicated. There is uptake in the region of para-aortic lymph nodes superimposed on the posterior liver and kidney outline and an edge artifact along the superior border of the liver.

ment. Kinetic analysis with probability mapping is a step in this direction which has been validated by comparison site by site with histology determined by biopsy in ovarian cancer.

APPENDIX 1

Computational Basis for Image Alignment and Kinetic Analysis Image Alignment

For each patient image, anterior or posterior, this image and the marker images were recorded as 128 × 128 matrices. Each marker image was analysed so that the site of maximum activity, the coordinates corresponding to the center of each marker, are computed using a correlation technique. The marker image B(i, j) is cross-correlated with a spot image A(i, j) formed from a two-dimensional normal density distribution. The normalized correlation measure used is defined as:

$$C(m,n) = \frac{\sum_{i=1}^{k}\sum_{j=1}^{k} A(i,j)\cdot B(m+i-k/2,\ n+j-k/2)}{\left[\sum_{i=1}^{k}\sum_{j=1}^{k} B^2\ (m+i-k/2,\ n+j-k/2)\right]}$$

For both images A(i, j) and B(i, j), the mean pixel count is subtracted from all pixel elements prior to correlation in order to enhance the sharpness of C(m, n). The locations of the maxima of C(m, n) yield the coordinates corresponding to the marker centres and correction for both translation and rotation is then made using the equations given below.

For images A and B, shift in the vertical and horizontal directions are given by $x = a_0 + x^1$ and $y = b_0 + y^1$. Image rotation through an angle θ is given by

$$x = a_1 x^1 + a_2 y^1$$
$$y = b_1 x^1 + b_2 y^1$$
$$a_1 = b_2 = \cos\theta$$
$$a_2 = b_1 = \sin\theta$$

The series of marker images are moved by a translation rotation program until the markers, that is the pixels with the most active points of the makers, are aligned. The images are then moved to a similar pattern. In this way repositioning of the images can be obtained accurately.

APPENDIX 2

Kinetic Analysis with Probability Mapping

The change detection algorithm is used to compare pairs of accurately spatially aligned images which have been obtained at different times after injection of the labeled antibody, for example the 10-min image, A, and the 22-hr image, B. Both images are scaled independently to a maximum pixel count of 256. The count rate content of each image is compared pixel by pixel as a frequency distribution, one image pixel's content being plotted on the x axis, the other on the y axis. For each count level, L, observed in image A, an average value Y_L is calculated for the N_L corresponding pixels in image B.

$$Y_L = S\cdot\frac{\sum_j Y_j}{N_L}, \text{ where S is the scaling factor for image B.}$$

For each value Y_L an associated weighted error W_L is calculated from the expression:

$$W_L = \left[\frac{S\cdot Y_L}{N_L}\right]^{1/2}$$

Comparison between the sets of pixel values defining the pair of aligned images is made using a weighted linear regression. A weighted least squares fit (LSF) of the linear expression: $Y_L = a + b.L$, is performed. Values of the coefficient of linear correlation R, standard error of the estimate, s.e.e., and the statistic formed by division of chi-squared by the degree of freedom X/N are calculated. Data with deviations from the fitted line greater than 1.2 s.e.e. (12% probability level) are rejected and a new LSF is carried out. In addition to values of R, s.e.e. and X/N, a value for the F ratio statistic is calculated.

$$F_N = \frac{[(N-1)\cdot X_{N-1} - N.X_N]}{X_N}$$

The F ratio is a measure of the fractional change in X/N occurring as a result of the reduction in the number of data points included in the LSF. A decrease in X/N indicates an improvement in the linear fit. This step of the method is repeated until no significant improvement in the linear fit is obtained as judged by a minimum in the F ratio. Assuming a normal distribution around this linear segment a probability map is constructed. For each individual pixel in image B, the deviation D of the count value from that predicted from the linear transformation is calculated and converted to a probability scale P based on the normal distribution. Three probability levels are mapped:

(i) $p < 0.001$, color coded red, corresponds to $D > 3.29$ s.e.e
(ii) $p < 0.01$, color coded yellow, corresponds to 2.58 s.e.e. $< D < 3.29$ s.e.e.
(iii) $p < 0.05$, color coded blue, corresponds to 1.96 s.e.e. $< D < 2.58$ s.e.e.

Additionally, in order to reduce the effect of random noise that is spatially distributed, a minimum cluster size K is defined for each probability level. So that the occasional abnormal pixel is excluded, the cluster definition requires that several pixels adjacent to each other are shown to be significantly different between the two images. Thus, if a pixel has less than K-1 adjacent pixels with the same probability level, it is downgraded to the next lower level of probability. Simulation studies show that noise artifacts are reduced if a signal to noise ratio over 20 is present at some location in the image and if a cluster size of five pixels is used. The technique can identify low contrast differences but in areas of low S/N value they may appear reduced in size. Detection of low contrast differences of ~10% may be influenced and improved by the presence of other regions of high contrast elsewhere in the image. Accurate pre-alignment of the images is essential or else edge artifacts may be formed. In summary, this change detection algorithm for kinetic analysis of serial image data with the demonstration of significant changes between the early and later images as a probability map meets the basic requirements of detectability of low contrast differences and insensitivity to statistical noise over the range encountered in a typical study.

ACKNOWLEDGMENTS

The authors thank the Imperial Cancer Research Fund laboratories for their financial support and for the supply of the HMFG2 antibody, and are grateful to St Bartholomew's Hospital Research Centre for the provision of laboratory facilities. The authors also thank Catherine Robinson for typing the manuscript.

REFERENCES

1. Granowska M, Britton KE, Crowther M, et al. Kinetic analysis with probability mapping in radioimmunoscintigraphy. In: Srivastava SC, eds. *Radiolabelled monoclonal antibodies for imaging and therapy.* NATO Advanced Study Institute: in press.
2. Taylor-Papadimitriou J, Peterson J, Arklie JA, et al. Monoclonal antibodies to epithelium-specific components of the human milk fat globule membrane: production and reaction with cells in culture. *Int J Cancer* 1981; 28: 17–21.
3. Arklie J, Taylor-Papadimitriou J, Bodmer WF, et al. Differentiation antigens expressed by epithelial cells in the lactating breast are also detectable in breast cancers. *Int J Cancer* 1981; 28: 23–29.
4. Burchell J, Durbin H, Taylor-Papadimitriou J. Complexity of expression of antigenic determinants, recognised by monoclonal antibodies HMFG-1 and HMFG-2, in normal and malignant human mammary epithelial cells. *J Immunol* 1983; 131: 509–513.
5. Shimuzu M, Yamauchi K. Isolation and characterisation of mucin-like glycoprotein in human milk fat globule membrane. *J Biochem* 1982; 91: 515–524.
6. Khan O, Cosgrove DO, Wiltshaw K, et al. Role of ultrasound in the management of ovarian carcinoma. *J Roy Soc Med* 1983; 76: 821–827.
7. Blaquiere RM, Husband JE. Conventional radiology and computed tomography in ovarian cancer [Discussion paper]. *J Roy Soc Med* 1983; 76: 574–579.
8. Granowska M, Shepherd J, Britton KE, et al. Ovarian cancer diagnosis using ^{123}I monoclonal antibody in comparison with surgical findings. *Nucl Med Commun* 1984; 5: 485–499.
9. Ott RJ, Grey LJ, Zivanovic MA. The limitations of the dual radionuclide subtraction technique for the external detection of tumours by radio-iodine-labelled antibodies. *Br J Radiol* 1983; 56: 101–108.
10. Granowska M, Britton KE, Shepherd JH, et al. A prospective study of I-123 labelled monoclonal antibody imaging in ovarian cancer. *J Clin Onc* 1986; 4: 730–736.
11. Granowska M, Britton KE, Shepherd J. The detection of ovarian cancer using 123-I monoclonal antibody. *Radiobiol Radiother* 1984; 25: 153–160.
12. Hammersmith Oncology Group: Antibody guided irradiation of malignant lesions: three cases illustrating a new method of treatment. *Lancet* 1984; 1: 1441–1443.
13. Britton KE, Granowska M, Mather S, et al. Experience with 123-I-labelled monoclonal antibodies. In: Donato L, Britton KE, eds. *Immunoscintigraphy.* Monographs in Nuclear Medicine, Vol I. Cox P ed, London: Gordon and Breach Science, 1985: 51–66.
14. Nimmon CC, Carroll MJ, Flatman W, et al. Spatial probability mapping of temporal change: application to gamma camera quality control and immunoscintigraphy [Abstract]. *Nucl Med Commun* 1984; 5: 231.